

Online Calibration Method for Pitch-Independent Laser Doppler Velocimeter Based on Improved Integrated Navigation Model

Zhiyi Xiang^{ID}, Qi Wang^{ID}, Rong Huang^{ID}, Shilong Jin^{ID}, Xiaoming Nie^{ID}, and Jian Zhou^{ID}

Abstract—The integrated navigation system, comprising a strapdown inertial navigation system (SINS) and a laser doppler velocimeter (LDV), is a promising solution for autonomous terrestrial navigation due to its high autonomy. Pitch-independent LDV (PI-LDV) is widely used because of its high-velocity measurement accuracy, small size, and independence from the vehicle pitch. However, the current use of PI-LDV is limited to the use of its 1-D velocity, neglecting the use of its two subvelocities. This article proposes three calibration models based on the two subvelocities of PI-LDV, which can obtain accurate 2-D velocity information of PI-LDV. First, a loosely integrated calibration model is proposed based on the traditional calibration model for PI-LDV and the 2-D velocity derived from the two subvelocities of PI-LDV. This model performs analytical coarse calibration before the filtering calibration. Second, a tightly integrated calibration model is proposed that directly estimates the error of the included angle between the two PI-LDV beams, since there is a strict mathematical relationship between the 2-D velocity and the included angle. Third, an ultratightly integrated calibration model is proposed that uses the two original beam measurements of the PI-LDV and introduces a third virtual beam information. Two groups of vehicle tests were carried out and the results verified that the accuracy of the corresponding integrated navigation of the three models proposed in this article is much better than the traditional scheme, especially in height estimation. Moreover, the ultratightly integrated calibration model has the best calibration effect among the three proposed models.

Index Terms—Calibration, integrated navigation, pitch-independent laser doppler velocimeter (PI-LDV), strapdown inertial navigation system (SINS), two-dimensional (2-D).

I. INTRODUCTION

DUCE to unavoidable initial alignment errors, installation errors, gyro drift, and accelerometer bias, the positioning error of strapdown inertial navigation system (SINS) will accumulate along with the time and show a trend of periodically oscillating divergence [1], [2]. To pursue higher navigation accuracy, the usual solution is to integrate SINS with other

Manuscript received 4 March 2023; revised 14 August 2023; accepted 30 August 2023. Date of publication 14 September 2023; date of current version 2 October 2023. This work was supported in part by the Major Basic Autonomous Research Project of the College of Advanced Interdisciplinary Studies; in part by the National University of Defense Technology under Grant ZDJC19-12; and in part by the Natural Science Foundation of Hunan Province, China, under Grant 2021JJ30782. The Associate Editor coordinating the review process was Dr. Alessio De Angelis. (*Corresponding author: Jian Zhou*)

The authors are with the College of Advanced Interdisciplinary Studies, Nanhua Laser Laboratory, National University of Defense Technology, Changsha 410073, China (e-mail: wttzhoujian@163.com).

Digital Object Identifier 10.1109/TIM.2023.3315425

sensors [3], [4], [5], [6], [7], [8]. The global positioning system (GPS) has been widely used for land navigation to mitigate the error drift of SINS, especially for low-cost SINS [9]. However, GPS is not always reliable in complex environments, such as wooded areas, urban canyons, and tunnels, where external signals are weak or unavailable. Since the odometer (OD) does not rely on external signals, SINS/OD integration is the most common terrestrial navigation mode in GPS-denied scenarios [10]. Unfortunately, the measurement result of OD depends on the wheel diameter and the rotation of the wheels, which are affected by the vehicle tire state and driving state. Therefore, the positioning accuracy of the SINS/OD-integrated navigation system is difficult to improve in practical applications [11].

Laser doppler velocimeter (LDV) is an ideal external velocity measurement sensor based on the optical Doppler effect. It has been widely used in various fields, such as biomedicine, fluid flow velocity measurement, meteorological observation, and others [12]. It has the advantages of high measurement accuracy, good spatial resolution, rapid dynamic response, wide speed measurement range, good directional sensitivity, and noncontact measurement [13], [14]. In recent years, LDV has been applied to the field of terrestrial navigation autonomously and many studies have demonstrated the effectiveness of SINS/LDV integration [15], [16], [17], [18], [19], [20]. Compared with the OD which directly measures the position increment of the vehicle, LDV directly measures the velocity of the vehicle, avoiding the information delay caused by unit transformation. In addition, when the LDV is rigidly mounted on the vehicle, the advantage of noncontact measurement of the LDV makes the measured value of the LDV immune to any elements associated with the wheels (such as tire temperature or pressure) as well as vehicle slipping and skidding [It should be noted that one-dimensional (1-D) and two-dimensional (2-D) LDV will not be able to avoid the impact of vehicle sideslip, but three-dimensional (3-D) LDV can solve this problem]. As the price of LDV decreases, LDV will be more widely used in the field of land vehicle autonomous navigation in the future.

In SINS/LDV-integrated navigation systems, there are angular misalignments between the LDV frame and the body frame, since the frame of the LDV is hard to coincide with the body frame. The errors also exist between the actual inclination angle of the LDV beam to the ground and the design value, which will lead to scale factor error.

To improve the accuracy of SINS/LDV-integrated navigation, it is imperative to calibrate the installation deviation between the LDV frame and body frame and the scale factor error of LDV accurately. In 2015, Zhang et al. [16] proposed an independent calibration method for SINS/1-D-LDV-integrated navigation system that uses the least squares algorithm and does not depend on any additional equipment or benchmarks. In 2017, a GPS-based high-precision calibration method was proposed in [1] to achieve high-precision calibration of SINS/1-D-LDV- and SINS/2-D-LDV-integrated navigation systems. This method divides the calibration process into two steps: analytic calibration and filtering calibration. In 2018, Wang et al. [21] introduces a split-reuse 3-D-LDV accurately calibrated its beam inclination error and installation misalignment angles using differential GPS. In addition, Wang et al. [22] also designed a 2-D-LDV and gave a calibration method for 2-D-LDV error parameters. To reduce the influence of LDV noise and GPS outliers on the calibration process, Xiang et al. [23] proposed a position observation-based calibration method for SINS/1-D-LDV-integrated navigation system. This method uses Davenport's q-method to estimate the misalignment angle matrix. Considering that GPS is not always reliable, Xi et al. [24] proposed a calibration method of SINS/1-D-LDV-integrated navigation system without GPS. This method uses highly accurate output information of the SINS in the early stage to carryout coarse calibration for the 1-D-LDV and then employs a Kalman filter to correct the results of coarse calibration to achieve high-precision calibration for the 1-D-LDV. Since the altitude information of SINS is divergent, this method cannot obtain the pitch installation misalignment angle of LDV.

Pitch-independent LDV (PI-LDV) is the most widely used LDV type today, due to its high precision, small size, and independence of the vehicle pitch. The PI-LDV can calculate the true velocity by using the two Doppler frequencies and the included angle between the two beams [12]. Besides, the highly accurate 1-D velocity output by PI-LDV, independent of the vehicle pitch, the 2-D velocity information can also be obtained by effectively using the two subvelocities of PI-LDV, which is expected to improve the height estimation accuracy of SINS/LDV-integrated navigation system. However, the current use of PI-LDV only utilizes its 1-D velocity, neglecting its two subvelocities, which does not fully exploit the advantages of PI-LDV [25], [26], [27], [28], [29].

To fully utilize the advantages of PI-LDV, this article proposes three calibration models based on the traditional GPS-assisted Kalman filter calibration method using the two subvelocities of PI-LDV. The first calibration model, called the loosely integrated calibration model, is based on the traditional calibration model for PI-LDV and the 2-D velocity derived from the two subvelocities of PI-LDV. This model divides the calibration process into two stages: coarse calibration and fine calibration. The second calibration model, called the tightly integrated calibration model, calibrates the included angle deviation between the two beams, which has different effects on the velocities in the two directions of PI-LDV. This model differs from the loosely integrated calibration model, which uses the same scale factor for both velocities of PI-LDV.

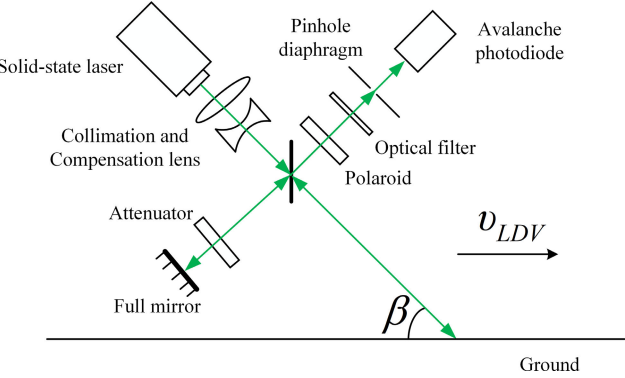


Fig. 1. Optical schematic of the traditional 1-D-LDV.

The third calibration model is called the ultratightly integrated calibration model. Compared with the loosely integrated calibration model and the tightly integrated calibration model, the ultratightly integrated calibration model directly uses the two beam measurements of the PI-LDV and introduces a third virtual beam measurement without transforming the two beam measurements of the PI-LDV to 2-D velocity, which will improve the robustness of the calibration process.

The rest of this article is organized as follows. In Section II, the traditional calibration model of PI-LDV is introduced. In Section III, three improved calibration models of PI-LDV are proposed. In Section IV, the proposed calibration models are compared with the traditional calibration model by using the vehicle-mounted field test data collected from PI-LDV-aided SINS. Concluding remarks are given in Section V.

II. REVIEW OF PI-LDV TRADITIONAL CALIBRATION MODEL

In this article, some important coordinate frames are defined: The local level navigation frame is denoted as the n frame (east–north–up). The body frame of SINS is denoted by b frame (right–forward–up). m frame represents the LDV frame. In this section, the m frame is rigidly fixed to the vehicle with the definition of right–forward–up.

The LDV measures velocity accurately by detecting the Doppler frequency shift of the light scattered by the ground. Fig. 1 shows the optical path structure of a traditional 1-D-LDV system. β is the inclination angle of the laser beam incident on the ground, and v_{LDV} is the velocity output of the 1-D-LDV, which is calculated by the following equation:

$$v_{LDV} = \lambda f_D / (2 \cos \beta) \quad (1)$$

where λ is the laser wavelength and f_D is the Doppler frequency.

Based on the traditional 1-D-LDV, a PI-LDV was proposed in the literature [12] to calculate the true velocity accurately using the two Doppler frequencies and the included angle between the two beams. At present, this PI-LDV, developed by our research group, has a measurement accuracy of better than 0.05% and has been successfully applied in the SINS/1-D-LDV-integrated navigation system. Fig. 2 shows the equipment diagram and beam direction of PI-LDV, and Fig. 3 illustrates its specific optical path structure. v_{beam1} and v_{beam2} are the

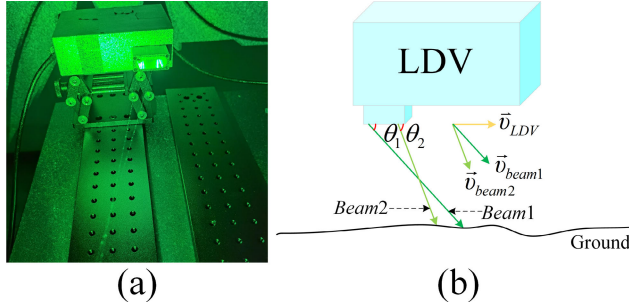


Fig. 2. (a) PI-LDV. (b) Beam direction of the PI-LDV.

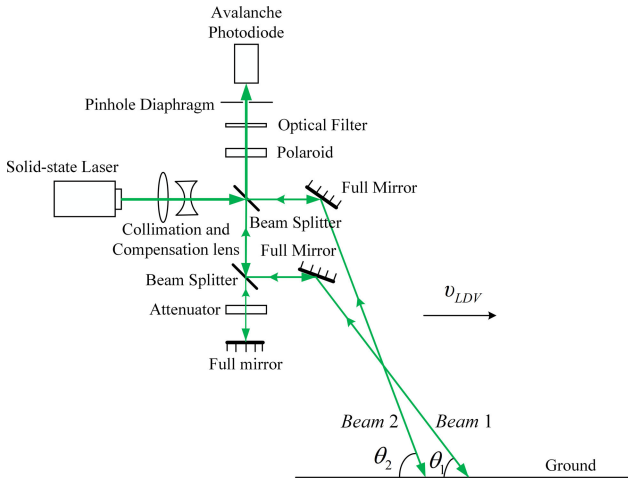


Fig. 3. Optical schematic of the PI-LDV.

two subvelocities of PI-LDV, θ_1 and θ_2 are the designed inclination angles of the two beams of PI-LDV. Different from the traditional 1-D-LDV, the 1-D velocity v_{LDV} output from PI-LDV is given by

$$v_{LDV} = \frac{\lambda f_{beam1}}{2} \sqrt{1 + \left(\frac{1}{\tan(2\Delta\theta)} - \frac{1}{\sin(2\Delta\theta)} \frac{f_{beam2}}{f_{beam1}} \right)^2} \quad (2)$$

where f_{beam1} and f_{beam2} are the Doppler frequencies measured by Beam 1 and Beam 2, $\Delta\theta = (\theta_2 - \theta_1)/2$.

A comparison of the angular parameters (β and $\Delta\theta$) in (1) and (2) shows that the 1-D velocity output of PI-LDV is independent of the pitch angle change of LDV. When the pitch angle of the LDV changes, the beam inclination angle β of traditional 1-D-LDV changes as well, while the beam inclination angles θ_1 and θ_2 of PI-LDV change simultaneously. Therefore, PI-LDV has a better performance than traditional 1-D-LDV.

Fig. 4 shows the block diagram of the traditional GPS-aided PI-LDV online calibration. ω_{ib}^b and f_{ib}^b are the gyro angular rate and the accelerometer specific force, respectively. v_{GPS} and p_{GPS} are the velocity and position outputs of the differential GPS, respectively.

When the PI-LDV only provides the 1-D velocity along the vehicle trajectory, the well-known nonholonomic constraints (NHC) of land vehicles can be used to realize 3-D velocity measurements. We denote the travel speed as v_y . The vehicle

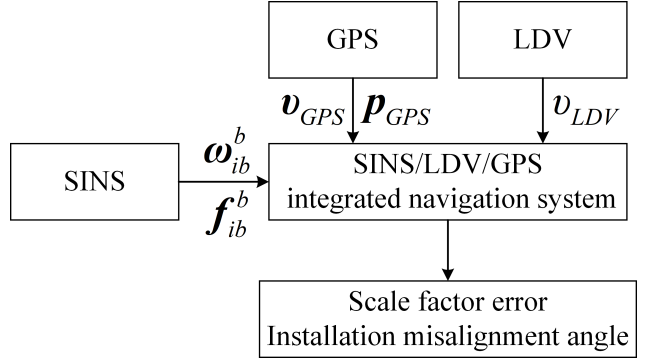


Fig. 4. Block diagram of traditional calibration model for the PI-LDV.

velocity in the m frame can be expressed as follows:

$$\mathbf{v}^m = [0 \quad v_y \quad 0]^T. \quad (3)$$

Due to the deviation between the actual inclination angle and the design inclination angle of PI-LDV, the vehicle velocity measured by PI-LDV in m frame is

$$\mathbf{v}_{LDV}^m = [0 \quad v_{LDV} \quad 0]^T = (1 + \delta K) \mathbf{v}^m \quad (4)$$

where δK represents the error in the scale factor due to the deviation of the beam inclination.

Based on (4) and the attitude output of the SINS, the velocity of PI-LDV in the n frame is

$$\mathbf{v}_{LDV}^n = \tilde{\mathbf{C}}_b^n \mathbf{C}_m^b \mathbf{v}_{LDV}^m = (\mathbf{I}_3 - \boldsymbol{\varphi} \times) \mathbf{C}_b^n (\mathbf{I}_3 - \boldsymbol{\phi}_m \times) (1 + \delta K) \mathbf{v}^m \quad (5)$$

where \mathbf{C}_b^n is the true attitude transfer matrix from the b frame to the n frame, $\boldsymbol{\varphi}$ is the attitude error of SINS, \mathbf{I}_3 is the 3×3 identity matrix, $\boldsymbol{\varphi} \times$ represents the antisymmetric matrix of $\boldsymbol{\varphi}$, \mathbf{C}_m^b is the installation misalignment matrix of m frame with respect to b frame, $\boldsymbol{\phi}_m$ is the installation misalignment angle of PI-LDV, $\boldsymbol{\phi}_m \times$ represents the antisymmetric matrix of $\boldsymbol{\phi}_m$, and $\tilde{\mathbf{C}}_b^n$ denote the error-contaminated attitude matrix.

According to (5), by omitting small quantities of the higher orders, the velocity error model of the PI-LDV is given as

$$\delta \mathbf{v}_{LDV}^n \approx (\mathbf{v}^n \times) \boldsymbol{\varphi} + \mathbf{C}_b^n (\mathbf{v}^m \times) \boldsymbol{\phi}_m + \delta K \mathbf{v}^m \quad (6)$$

where \mathbf{v}^n denotes the vehicle true velocity in the n frame and $\mathbf{v}^m \times$ is the antisymmetric matrix of \mathbf{v}^m .

Given that the PI-LDV has excellent performance and its installation relationship with the SINS is fixed, the corresponding scale factor error and installation misalignment angle can be treated as random constants so that the following error equation can be obtained:

$$\begin{aligned} \delta \dot{K} &= 0 \\ \dot{\phi}_{mx} &= 0 \\ \dot{\phi}_{mz} &= 0 \end{aligned} \quad (7)$$

where ϕ_{mx} and ϕ_{mz} are the pitch installation misalignment angle and the heading installation misalignment angle of PI-LDV, respectively (The 1-D velocity of the LDV output is not affected by the LDV roll installation misalignment angle).

The state equations of the PI-LDV traditional calibration model can be derived based on the error equations of SINS and (7), and then the measurement equations of the PI-LDV traditional calibration model can be obtained based on (6) as well as the velocity and position outputs of SINS and GNSS, and finally the PI-LDV can be calibrated by the Kalman filter algorithm.

For the traditional calibration model of PI-LDV and the traditional SINS/PI-LDV-integrated navigation system, there is a problem that the upward velocity of PI-LDV is based on the NHC assumption, which is not fully satisfied in most cases. The actual vertical zero velocity constraint is not aligned with the upward axis of the m frame, but with the normal vector of the road surface. Therefore, for the traditional SINS/PI-LDV-integrated navigation system, the pitch installation misalignment angle actually represents the pitch relationship between inertial measurement unit (IMU) and road. In practical applications, changes in load, tire pressure, and road conditions will cause changes in the pitch installation misalignment angle, which is also the fundamental reason why the traditional calibration model of PI-LDV cannot calibrate the pitch installation misalignment angle accurately and the traditional SINS/PI-LDV-integrated navigation system cannot maintain a high height accuracy for a long time.

III. PROPOSED PI-LDV CALIBRATION MODEL

Compared to the 1-D-LDV, the 2-D-LDV can directly measure the upward velocity of the vehicle without the need for relying on the NHC assumption, which allows the SINS/2-D-LDV-integrated navigation system to obtain height information that is superior to that of the SINS/1-D-LDV-integrated navigation system. As Fig. 3 illustrates, the two measurement beams of the PI-LDV intersect, enabling 2-D velocity information to be obtained by using the two subvelocities along the beam direction. However, the current applications of PI-LDV only utilize its 1-D velocity, which does not fully exploit its advantage in optical path structure. To achieve this, the two subvelocities of PI-LDV must be fully used, which requires a reasonable modeling and an accurate calibration of PI-LDV to obtain an accurate 2-D velocity. In this section, three calibration models are proposed based on the traditional GPS-assisted Kalman filter calibration method using the two subvelocities of PI-LDV.

A. Proposed Loosely Integrated Calibration Model

Based on the traditional calibration model, this subsection proposes a loosely integrated calibration model from the two subvelocities of PI-LDV. In the loosely integrated calibration model, the m frame is established as follows: the direction with an angle of θ_2 to the second incident beam is taken as the Y_m axis and the forward direction is positive, the vertical line of Y_m axis in the plane of the two incident beams is Z_m axis and the upward direction is positive, and the X_m axis is determined by the right-hand rule. The installation relationship of PI-LDV and IMU and the coordinate system relationship in the loosely integrated calibration model are shown in Fig. 5.

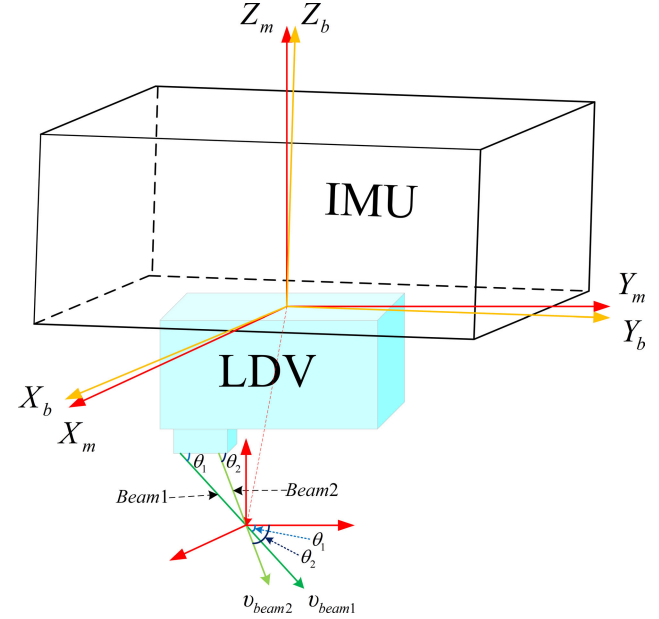


Fig. 5. Installation relationship of the PI-LDV and IMU and the coordinate system relationship in the loosely integrated calibration model.

As shown in Fig. 5, the forward and vertical velocities of the PI-LDV in the m frame are related to the two subvelocities of the PI-LDV by the following deterministic relationship:

$$v_{LDV-y} = \frac{v_{beam2} \sin \theta_1 - v_{beam1} \sin \theta_2}{\sin \theta_1 \cos \theta_2 - \cos \theta_1 \sin \theta_2} \quad (8)$$

$$v_{LDV-z} = \frac{v_{beam1} \cos \theta_2 - v_{beam2} \cos \theta_1}{\sin \theta_1 \cos \theta_2 - \cos \theta_1 \sin \theta_2} \quad (9)$$

where v_{LDV-y} and v_{LDV-z} are the forward and vertical velocities of the PI-LDV in the m frame, respectively. The (8) and (9) can be obtained by solving the following equations:

$$v_{LDV-y} \cos \theta_1 + v_{LDV-z} \sin \theta_1 = v_{beam1} \quad (10)$$

$$v_{LDV-y} \cos \theta_2 + v_{LDV-z} \sin \theta_2 = v_{beam2}. \quad (11)$$

When the PI-LDV provides information of two subvelocities, the forward and vertical velocities of the vehicle can be obtained from the two subvelocities of the PI-LDV, so the assumption that the vertical velocity is zero in the traditional calibration method will no longer be appropriate. Equation (3) is rewritten as

$$\mathbf{v}^m = [0 \quad v_y \quad v_z]^T \quad (12)$$

where v_z is the vertical velocity in the m frame.

Since the included angle between the first incident beam and the Y_m axis has a slight deviation from θ_1 which leads to scale factor error, the measured vehicle velocity of PI-LDV in the m frame is

$$\mathbf{v}_{LDV}^m = [0 \quad v_{LDV-y} \quad v_{LDV-z}]^T = (1 + \delta K) \mathbf{v}^m. \quad (13)$$

In the loosely integrated calibration model, the analytical method is used as the coarse calibration. Gao et al. [1] suggest that a coarse calibration before filter calibration can improve the accuracy of the calibration and applies the analytical method as the coarse calibration method. However, it does not perform the coarse calibration of the pitch installation

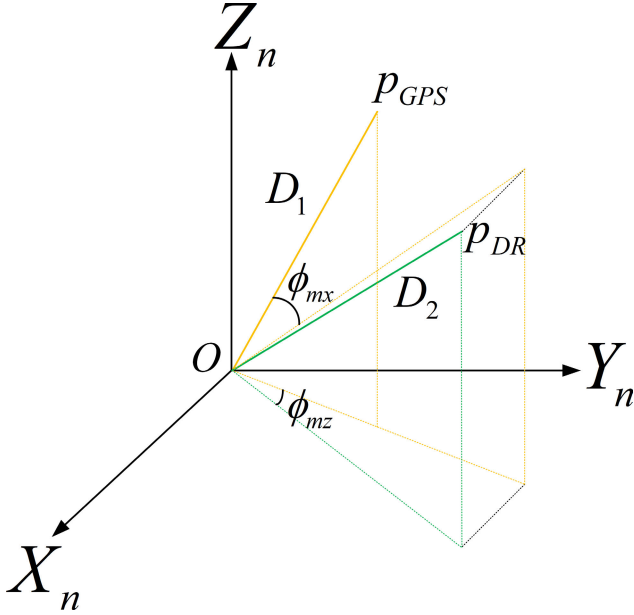


Fig. 6. Schematic of the relationship between GPS trajectory and DR trajectory.

misalignment angle. To fully utilize PI-LDV's advantage in height estimation, a coarse calibration of this angle is essential. Fig. 6 shows the relationship between the GPS trajectory and the SINS/PI-LDV dead reckoning (DR) trajectory at the initial time in the n frame. Point O indicates the initial position of the vehicle, and its coordinate is (X_O, Y_O, Z_O) . Points p_{GPS} and p_{DR} represent the GPS position and SINS/PI-LDV DR position of the vehicle after a short period of motion, and their coordinates are $(X_{GPS}, Y_{GPS}, Z_{GPS})$ and (X_{DR}, Y_{DR}, Z_{DR}) , respectively. D_1 is the distance between O and p_{GPS} , and D_2 is the distance between O and p_{DR} .

According to Fig. 6, the coarse calibration results for the scale factor and the installation misalignment angles are

$$K_{LDV} = \frac{D_1}{D_2} \quad (14)$$

$$\phi_{mx} = a \sin\left(\frac{Z_{GPS} - Z_O}{D_1}\right) - a \sin\left(\frac{Z_{DR} - Z_O}{D_2}\right) \quad (15)$$

$$\phi_{mz} = a \tan\left(\frac{Y_{GPS} - Y_O}{X_{GPS} - X_O}\right) - a \tan\left(\frac{Y_{DR} - Y_O}{X_{DR} - X_O}\right). \quad (16)$$

Based on the coarse calibration results, (5) and (6) can be rewritten as

$$\mathbf{v}_{LDV}^n = (\mathbf{I}_3 - \boldsymbol{\varphi} \times) \mathbf{C}_b^n (\mathbf{I}_3 - \boldsymbol{\phi}'_m \times) \mathbf{v}_{LDV}^{m'} \quad (17)$$

$$\delta \mathbf{v}_{LDV}^n \approx (\mathbf{v}^n \times) \boldsymbol{\varphi} + \mathbf{C}_b^n (\mathbf{v}^{m'} \times) \boldsymbol{\phi}'_m + \delta K' \mathbf{v}^n \quad (18)$$

where the m' frame represents the LDV frame after the coarse calibration is completed, $\delta K'$ is the scale factor error after the completion of the coarse calibration, and $\boldsymbol{\phi}'_m$ denotes the installation misalignment angle of PI-LDV after the coarse calibration is completed. $\mathbf{v}^{m'}$ represents the vehicle true velocity in the m' frame. The measured vehicle velocity of PI-LDV in the m' frame is

$$\begin{aligned} \mathbf{v}_{LDV}^{m'} &= K_{LDV} \mathbf{C}_m^{m'} \mathbf{v}_{LDV}^m = (1 + \delta K) K_{LDV} \mathbf{C}_m^m \mathbf{v}^m \\ &= (1 + \delta K') \mathbf{v}^{m'} \end{aligned} \quad (19)$$

where $\mathbf{C}_m^{m'}$ is the transformation matrix from the m frame to the m' frame.

After the coarse calibration, a fine calibration of PI-LDV is performed by using the Kalman filter. Since the 2-D velocity of PI-LDV is used, the roll installation misalignment angle will be considered in the proposed loosely integrated calibration model. The error equation of the PI-LDV error parameter is

$$\begin{aligned} \delta \dot{K}' &= 0 \\ \dot{\phi}'_{mx} &= 0 \\ \dot{\phi}'_{my} &= 0 \\ \dot{\phi}'_{mz} &= 0 \end{aligned} \quad (20)$$

where $\dot{\phi}'_{mx}$, $\dot{\phi}'_{my}$, and $\dot{\phi}'_{mz}$ are the pitch installation misalignment angle, roll installation misalignment angle, and the heading installation misalignment angle of PI-LDV after the coarse calibration is completed, respectively.

The state equation of the proposed loosely integrated calibration model is given as

$$\dot{\mathbf{x}} = \mathbf{F}\mathbf{x} + \mathbf{G}\mathbf{w} \quad (21)$$

where \mathbf{F} is the 19×19 system state transition matrix, \mathbf{G} is the noise transfer matrix, and \mathbf{w} is the system noise vector. \mathbf{x} is the 19-D state vector and can be written as

$$\mathbf{x} = [\mathbf{x}_{SINS}^T \quad \mathbf{x}_{LDV}^T]^T \quad (22)$$

$$\mathbf{x}_{SINS} = [\boldsymbol{\varphi}^T \quad (\delta \mathbf{v}_{SINS}^n)^T \quad (\delta \mathbf{p}_{SINS})^T \quad (\boldsymbol{\epsilon}_{ib}^b)^T \quad (\nabla_{ib}^b)^T]^T \quad (23)$$

$$\mathbf{x}_{LDV} = [\phi'_{mx} \quad \phi'_{my} \quad \phi'_{mz} \quad \delta K']^T \quad (24)$$

where $\delta \mathbf{v}_{SINS}^n$ and $\delta \mathbf{p}_{SINS}$ are the velocity error and position error of SINS, respectively.

The matrices \mathbf{F} and \mathbf{G} can be decomposed as

$$\mathbf{F} = \begin{bmatrix} \mathbf{F}_{SINS} & \mathbf{0}_{15 \times 4} \\ \mathbf{0}_{4 \times 15} & \mathbf{0}_{4 \times 4} \end{bmatrix} \quad (25)$$

$$\mathbf{G} = \begin{bmatrix} -\mathbf{C}_b^n & \mathbf{0}_{3 \times 3} \\ \mathbf{0}_{3 \times 3} & \mathbf{C}_b^n \\ \mathbf{0}_{13 \times 3} & \mathbf{0}_{13 \times 3} \end{bmatrix} \quad (26)$$

where \mathbf{F}_{SINS} is a 15×15 state transition matrix based on the classic SINS error model [30].

The system noise vector can be expressed as

$$\mathbf{w}(t) = [\varepsilon_{wx} \quad \varepsilon_{wy} \quad \varepsilon_{wz} \quad \nabla_{wx} \quad \nabla_{wy} \quad \nabla_{wz}]^T \quad (27)$$

where ε_{wi} and ∇_{wi} ($i = x, y, z$) denote the noise of the gyro and accelerometer, respectively.

The established measurement equation is

$$\mathbf{z} = \begin{bmatrix} \mathbf{v}_{SINS}^n - \mathbf{v}_{GPS} \\ \mathbf{p}_{SINS} - \mathbf{p}_{GPS} \\ \mathbf{v}_{LDV}^n - \mathbf{v}_{GPS} \end{bmatrix} = \mathbf{H}\mathbf{x} + \mathbf{v} \quad (28)$$

where \mathbf{H} is the measurement transition matrix, \mathbf{v} is the measurement noise (zero-mean Gaussian white noise), and \mathbf{z} is the measurement value. \mathbf{v}_{SINS}^n and \mathbf{p}_{SINS} are the velocity output and position output of SINS, respectively. \mathbf{v}_{GPS} and \mathbf{p}_{GPS} are the velocity output and position output of GPS, respectively.

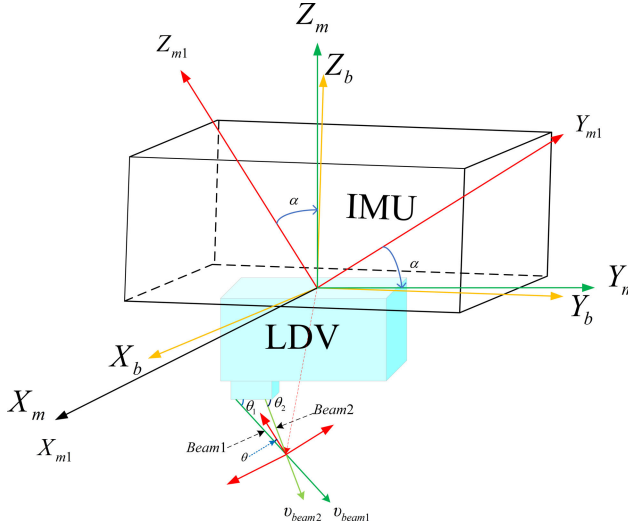


Fig. 7. Installation relationship of the PI-LDV and IMU and the coordinate system relationship in the tightly integrated calibration model.

According to (18) and (22), the measurement transition matrix \mathbf{H} can be expressed as

$$\mathbf{H} = \begin{bmatrix} \mathbf{0}_{6 \times 3} & \mathbf{I}_6 & \mathbf{0}_{6 \times 6} & \mathbf{0}_{6 \times 3} & \mathbf{0}_{6 \times 1} \\ \mathbf{v}^n \times & \mathbf{0}_{3 \times 6} & \mathbf{0}_{3 \times 6} & \mathbf{C}_b^n (\mathbf{v}^{m'} \times) & \mathbf{v}^n \end{bmatrix}. \quad (29)$$

B. Proposed Tightly Integrated Calibration Model

In the loosely integrated calibration model, the scale factor error in the two directions of PI-LDV is assumed to be identical. However, this assumption may not be appropriate, since the beam inclination angle error affects the forward and vertical velocities differently. To address this issue, this subsection proposes a tightly integrated calibration model. In this model, the deviation of the included angle between two beams is directly estimated. Fig. 7 shows the installation relationship between IMU and PI-LDV and the coordinate system relationship in the tightly integrated calibration model.

In Fig. 7, X_{m1} , Y_{m1} , and Z_{m1} are three axes of the initial frame of the PI-LDV ($m1$ frame), and the $m1$ frame is established as follows: the angle bisector of the two incident beams is taken as Z_{m1} axis and the upward direction is positive, the vertical line of Z_{m1} axis in the plane of the two incident beams is Y_{m1} axis and the forward direction is positive, and the X_{m1} is determined by the right hand rule. θ is the included angle between the angle bisector of the two incident beams and two incident beams. The m frame is obtained by rotating the $m1$ frame clockwise around the X_{m1} axis by a constant angle α .

As shown in Fig. 7, the forward and vertical velocities of the PI-LDV in the $m1$ frame are related to the two subvelocities of the PI-LDV by following deterministic relationships:

$$v'_{\text{LDV}-y} = \frac{v_{\text{beam}1} - v_{\text{beam}2}}{2 \sin \theta} \quad (30)$$

$$v'_{\text{LDV}-z} = \frac{-(v_{\text{beam}1} + v_{\text{beam}2})}{2 \cos \theta} \quad (31)$$

where the (30) and (31) can be obtained by solving the following equations:

$$v'_{\text{LDV}-y} \sin \theta - v'_{\text{LDV}-z} \cos \theta = v_{\text{beam}1} \quad (32)$$

$$-v'_{\text{LDV}-y} \sin \theta - v'_{\text{LDV}-z} \cos \theta = v_{\text{beam}2}. \quad (33)$$

Since there is a deviation of θ from the true value, the measured vehicle velocity of PI-LDV in the $m1$ frame and m frame can be written as

$$\begin{aligned} \mathbf{v}_{\text{LDV}}^{m1} &= [0 \quad v'_{\text{LDV}-y} \quad v'_{\text{LDV}-z}]^T \\ &= \mathbf{v}^{m1} + \begin{bmatrix} 0 \\ -v'_{\text{LDV}-y} \cot \theta \\ v'_{\text{LDV}-z} \tan \theta \end{bmatrix} \Delta \theta \end{aligned} \quad (34)$$

$$\begin{aligned} \mathbf{v}_{\text{LDV}}^m &= \mathbf{C}_{\alpha x} \mathbf{v}_{\text{LDV}}^{m1} = \mathbf{v}^m + \mathbf{C}_{\alpha x} \begin{bmatrix} 0 \\ -v'_{\text{LDV}-y} \cot \theta \\ v'_{\text{LDV}-z} \tan \theta \end{bmatrix} \Delta \theta \\ &= \mathbf{v}^m + \mathbf{C}_{\alpha x} \mathbf{C}_{\theta} \Delta \theta \end{aligned} \quad (35)$$

where \mathbf{v}^{m1} is the vehicle velocity in the $m1$ frame and $\Delta \theta$ is the error of the θ .

$$\begin{aligned} \mathbf{C}_{\theta} &= [0 \quad -v'_{\text{LDV}-y} \cot \theta \quad v'_{\text{LDV}-z} \tan \theta]^T \\ \mathbf{C}_{\alpha x} &= \begin{bmatrix} 1 & 0 & 0 \\ 0 & \cos \alpha & -\sin \alpha \\ 0 & \sin \alpha & \cos \alpha \end{bmatrix}. \end{aligned}$$

According to (35), the velocity and velocity error model of PI-LDV in the n frame is

$$\mathbf{v}_{\text{LDV}}^n = (\mathbf{I}_3 - \boldsymbol{\varphi} \times) \mathbf{C}_b^n (\mathbf{I}_3 - \boldsymbol{\phi}_m \times) (\mathbf{v}^m + \mathbf{C}_{\alpha x} \mathbf{C}_{\theta} \Delta \theta) \quad (36)$$

$$\delta \mathbf{v}_{\text{LDV}}^n \approx (\mathbf{v}^n \times) \boldsymbol{\varphi} + \mathbf{C}_b^n (\mathbf{v}^m \times) \boldsymbol{\phi}_m + \mathbf{C}_b^n \mathbf{C}_{\alpha x} \mathbf{C}_{\theta} \Delta \theta. \quad (37)$$

The state vector contains 19 variables and is expressed as follows:

$$\mathbf{x} = [\mathbf{x}_{\text{SINS}}^T \quad \mathbf{x}_{\text{LDV}}^T]^T \quad (38)$$

$$\mathbf{x}_{\text{SINS}} = [\boldsymbol{\varphi}^T \quad (\delta \mathbf{v}_{\text{SINS}}^n)^T \quad (\delta \mathbf{p}_{\text{SINS}})^T \quad (\boldsymbol{\varepsilon}_{ib}^b)^T \quad (\nabla_{ib}^b)^T]^T \quad (39)$$

$$\mathbf{x}_{\text{LDV}} = [\phi_{mx} \quad \phi_{my} \quad \phi_{mz} \quad \Delta \theta]^T. \quad (40)$$

Since $\Delta \theta$ still satisfies the condition that its derivative is zero, the system state transition matrix \mathbf{F} and noise transfer matrix \mathbf{G} are consistent with equations (25) and (26).

According to the measurement equation in (28) and the new velocity error model of the PI-LDV in (37), the measurement transition matrix \mathbf{H} can be obtained as

$$\mathbf{H} = \begin{bmatrix} \mathbf{0}_{6 \times 3} & \mathbf{I}_6 & \mathbf{0}_{6 \times 6} & \mathbf{0}_{6 \times 3} & \mathbf{0}_{6 \times 1} \\ \mathbf{v}^n \times & \mathbf{0}_{3 \times 6} & \mathbf{0}_{3 \times 6} & \mathbf{C}_b^n (\mathbf{v}^m \times) & \mathbf{C}_b^n \mathbf{C}_{\alpha x} \mathbf{C}_{\theta} \end{bmatrix}. \quad (41)$$

C. Proposed Ultratightly Integrated Calibration Model

Under complex road conditions, some beam measurement values of PI-LDV may be inaccurate or unavailable, which can cause large errors in the 2-D velocity obtained by the two beam measurement values of PI-LDV. This can significantly reduce the calibration accuracy of the PI-LDV. To improve the robustness of the calibration process, this subsection proposes

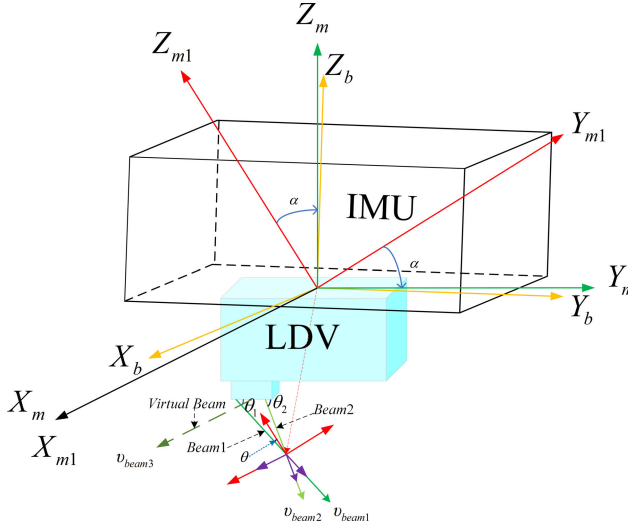


Fig. 8. Installation relationship of the PI-LDV and IMU and the coordinate system relationship in the ultratightly integrated calibration model.

an ultratightly integrated calibration model that uses the two subvelocities of PI-LDV directly without transforming them into 2-D velocity. Moreover, a virtual beam along the X_m axis direction is added as a lateral constraint to enhance calibration accuracy. The definition of the coordinate frame is consistent with that in the tightly integrated calibration model. Fig. 8 illustrates the installation relationship between IMU and PI-LDV and the coordinate system relationship in the ultratightly integrated calibration model. v_{beam3} is the velocity along the direction of the virtual beam, and $v_{beam3} = 0$.

According to (32), (33), and Fig. 8, the conversion relationship between the beam frame and the m frame can be expressed as follows:

$$\begin{bmatrix} v_{beam1} \\ v_{beam2} \\ v_{beam3} \end{bmatrix} = v_{LDV}^{\text{beam}} = C_{m1}^{\text{beam}} C_{\alpha x}^T v_{LDV}^m \quad (42)$$

where

$$\begin{aligned} C_{m1}^{\text{beam}} &= \begin{bmatrix} 0 & \sin \theta & -\cos \theta \\ 0 & -\sin \theta & -\cos \theta \\ 1 & 0 & 0 \end{bmatrix} \\ &+ \begin{bmatrix} 0 & \cos \theta & \sin \theta \\ 0 & -\cos \theta & \sin \theta \\ 0 & 0 & 0 \end{bmatrix} \Delta \theta \\ &= C_B + C_{dB} \Delta \theta. \end{aligned} \quad (43)$$

Based on the conversion relationship described in (42), the projection of the GPS velocity in the beam frame is given by

$$v_{GPS}^{\text{beam}} = C_{m1}^{\text{beam}} C_{\alpha x}^T (I_3 + \phi_m \times) C_n^b (I_3 + \varphi \times) v_{GPS}. \quad (44)$$

The SINS/PI-LDV ultratightly integrated calibration model is established based on the two-beam channel velocity information of the PI-LDV and the virtual beam velocity information of the PI-LDV. The state vector \mathbf{x} , the system state transition matrix \mathbf{F} , and the noise transfer matrix \mathbf{G} remain consistent with those in the tightly integrated calibration model.

TABLE I
COMPARISON BETWEEN DIFFERENT CALIBRATION MODELS FOR PI-LDV

Model	Calibrated PI-LDV Dimension	Calibration Method	Calibration Parameter	Measurement Equation
Traditional	1D	Kalman Filter	$\phi_m, \delta K$	$v_{SINS}^n - v_{GPS}$ $p_{SINS} - p_{GPS}$ $v_{LDV}^n - v_{GPS}$
Loosely Integrated	2D	Analytical Method, Kalman Filter	$\phi_m, \delta K$	$v_{SINS}^n - v_{GPS}$ $p_{SINS} - p_{GPS}$ $v_{LDV}^n - v_{GPS}$
Tightly Integrated	2D	Kalman Filter	$\phi_m, \Delta \theta$	$v_{SINS}^n - v_{GPS}$ $p_{SINS} - p_{GPS}$ $v_{LDV}^n - v_{GPS}$
Ultra-Tightly Integrated	2D	Kalman Filter	$\phi_m, \Delta \theta$	$v_{SINS}^n - v_{GPS}$ $p_{SINS} - p_{GPS}$ $v_{beam}^{\text{beam}} - v_{beam}^{\text{GPS}}$ $v_{LDV}^{\text{beam}} - v_{beam}^{\text{GPS}}$

The measurement equation is established as follows:

$$\mathbf{z} = \begin{bmatrix} v_{SINS}^n - v_{GPS} \\ p_{SINS} - p_{GPS} \\ v_{LDV}^{\text{beam}} - v_{beam}^{\text{GPS}} \end{bmatrix} = \mathbf{Hx} + \mathbf{v} \quad (45)$$

where

$$v_{LDV}^{\text{beam}} - v_{beam}^{\text{GPS}} \approx \mathbf{C}_B \mathbf{C}_{\alpha x}^T \mathbf{C}_n^b (v_{GPS} \times) \boldsymbol{\varphi} + \mathbf{C}_B \mathbf{C}_{\alpha x}^T (v_{GPS}^b \times) \boldsymbol{\phi}_m - \mathbf{C}_{dB} \mathbf{C}_{\alpha x}^T \mathbf{C}_n^b v_{GPS} \Delta \theta \quad (46)$$

where v_{GPS}^b is the projection of the GPS output velocity in the b frame.

According to state vector and (46), we can derive the measurement transition matrix \mathbf{H} as follows:

$$\mathbf{H} = \begin{bmatrix} \mathbf{0}_{6 \times 3} & \mathbf{C}_B \mathbf{C}_{\alpha x}^T \mathbf{C}_n^b (v_{GPS} \times) \\ \mathbf{I}_6 & \mathbf{0}_{3 \times 6} \\ \mathbf{0}_{6 \times 6} & \mathbf{0}_{3 \times 6} \\ \mathbf{0}_{6 \times 3} & \mathbf{C}_B \mathbf{C}_{\alpha x}^T (v_{GPS}^b \times) \\ \mathbf{0}_{6 \times 1} & -\mathbf{C}_{dB} \mathbf{C}_{\alpha x}^T \mathbf{C}_n^b v_{GPS} \end{bmatrix}^T. \quad (47)$$

D. Analyzation for Different Calibration Model

The comparison between different calibration models for PI-LDV is summarized in Table I. Compared with the traditional calibration models, the three calibration models proposed in this article enable the PI-LDV to obtain accurate 2-D information, which makes the vertical velocity of the PI-LDV in its own frame does not need to use NHC assumption, and thus improves the calibration accuracy of the pitch installation misalignment angle and the height estimation accuracy of the SINS/PI-LDV-integrated navigation system. The loosely integrated calibration model divides the calibration process into analytical coarse calibration and filtering fine calibration, which can improve the convergence speed of the calibration process. However, this model still follows the method in the traditional calibration model, which attributes the effect of the beam inclination angle error to one scale factor

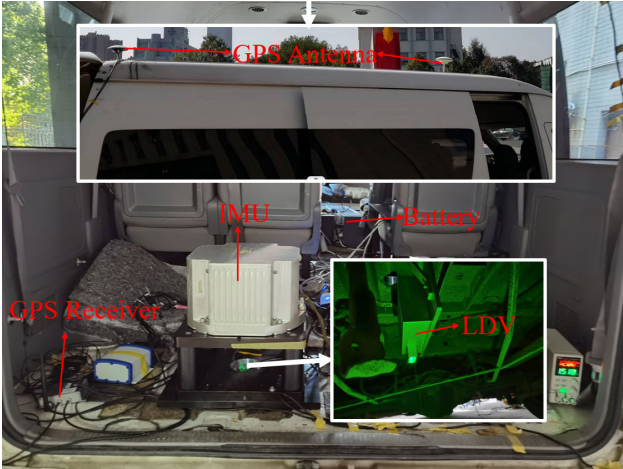


Fig. 9. Installation diagram of the experimental system.

error. This is unreasonable for the modeling of the 2-D-LDV, since the effect of the beam inclination angle error on the forward and vertical velocities is different. This greatly limits the calibration accuracy of the loosely integrated calibration model. In contrast, both the tightly integrated calibration model and the ultratightly integrated calibration model directly estimate the deviation of the angle between the two beams of PI-LDV. Since the forward and vertical velocities obtained from PI-LDV are directly related to this angle, these models have higher accuracy than the loosely integrated calibration model. Compared with the tightly integrated calibration model, the ultratightly integrated calibration model directly uses the subvelocities measured by each of the two PI-LDV beams instead of transforming them to 2-D velocities, and introduces a virtual beam with a constant zero output along the X_m axis as a lateral constraint. This way, the ultratightly integrated calibration model can still work properly even if one of the subvelocities fails temporarily without diverging rapidly. Thus, this model has higher robustness than the tightly integrated calibration model.

IV. VEHICLE TEST

To verify the validity of the model proposed in this article, two groups of vehicle-mounted tests were conducted. Fig. 9 shows the test equipment, which includes a self-developed IMU, a self-made PI-LDV, and a dual-antenna differential GPS receiver. The IMU consists of three-ring laser gyros and three quartz accelerometers with an output frequency of 100 Hz. The gyros have a bias instability within $0.007^\circ/\text{h}$ and a random walk within $0.001^\circ/\sqrt{\text{h}}$. The accelerometers have a bias instability within $50 \mu\text{g}$ and a random walk of $50 \mu\text{g}/\sqrt{\text{h}}$. The PI-LDV has a velocity measurement error within 0.1% (1σ) with an output frequency of 100 Hz. The GPS has a horizontal positioning accuracy and an altitude accuracy within 0.05 m with an output frequency of 10 Hz.

Two groups of field tests were conducted in Changsha City. The vehicle remained stationary for about 13 min at the start point before moving. During this time, a static attitude alignment was performed to obtain an accurate initial attitude.

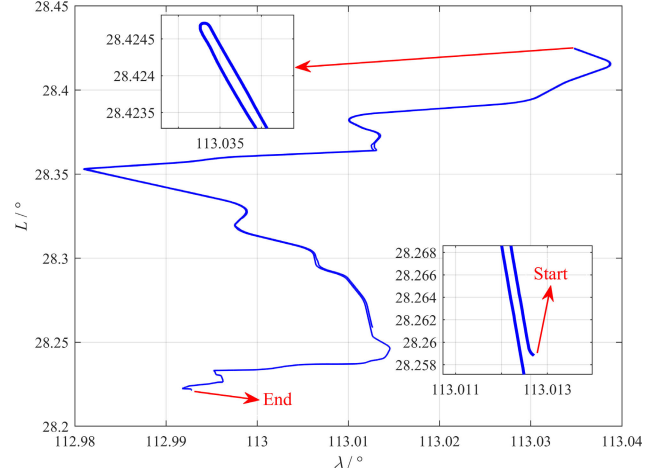


Fig. 10. Trajectory of the vehicle in the first field test.

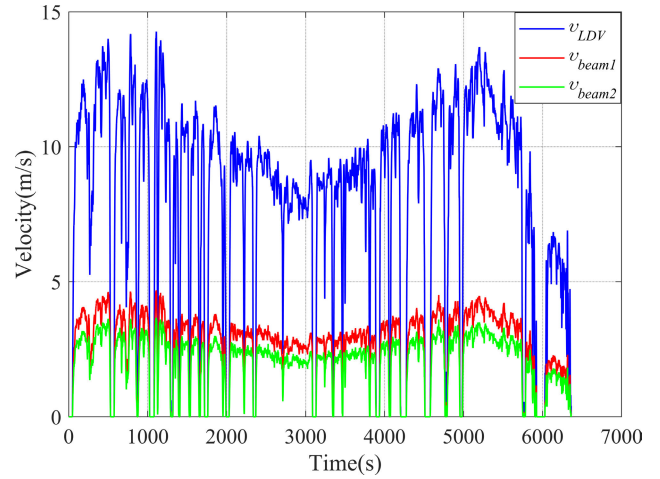


Fig. 11. Velocity curve of PI-LDV output in the first field test.

To evaluate the calibration performance of the proposed model, the following four models are defined for comparison.

Model 1: The traditional calibration model for PI-LDV introduced in Section II.

Model 2: The loosely integrated calibration model for PI-LDV proposed in Section III-A.

Model 3: The tightly integrated calibration model for PI-LDV proposed in Section III-B.

Model 4: The ultratightly integrated calibration model for PI-LDV proposed in Section III-C.

The movement trajectory and the PI-LDV measurement output from the first vehicle test are shown in Figs. 10 and 11, respectively. First, the traditional calibration model for PI-LDV introduced in this article is applied for calibration processing and the results are shown in Fig. 12. Second, the loosely integrated calibration model for PI-LDV proposed in this article is used for calibration processing and the results are shown in Fig. 13. Third, both the tightly integrated and ultratightly integrated calibration models for PI-LDV proposed in this article are performed for calibration processing and the results are shown in Figs. 14–17.

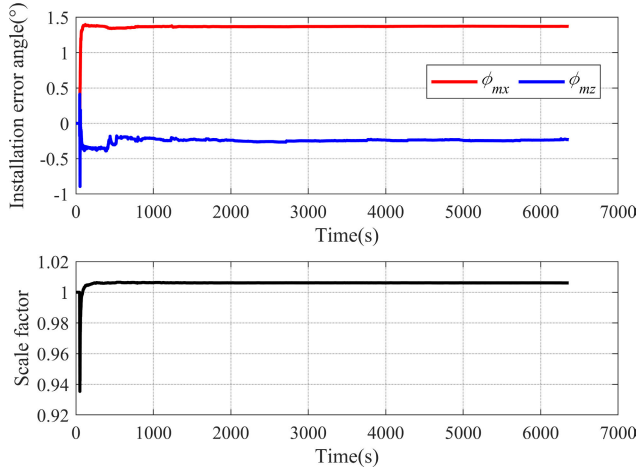


Fig. 12. Calibration results for the traditional calibration model in the first field test.

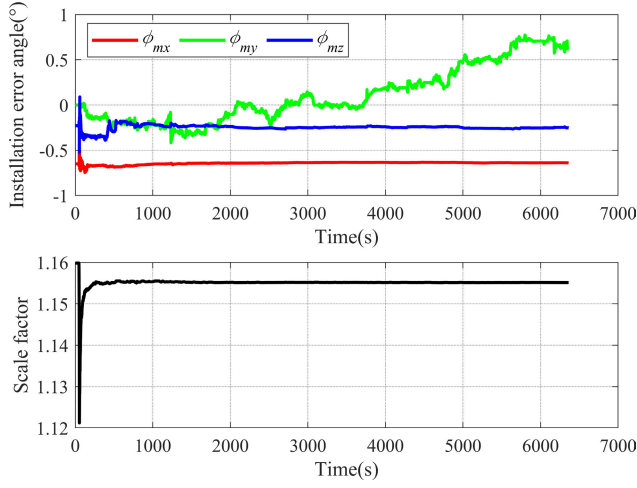


Fig. 13. Calibration results for the loosely integrated calibration model in the first field test.

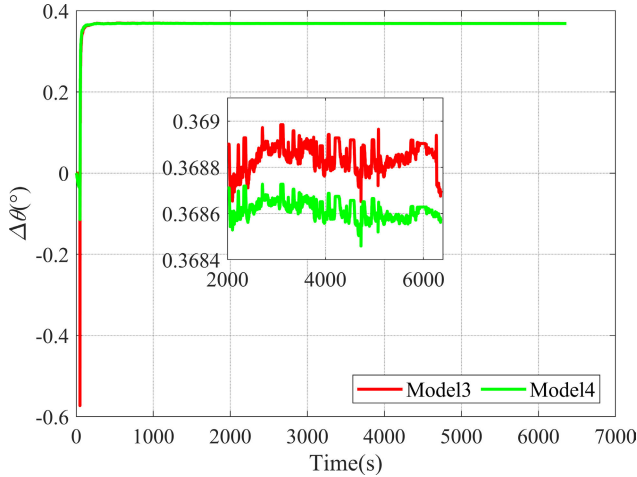


Fig. 14. Curve of the $\Delta\theta$ for the tightly integrated calibration model and the ultratightly integrated calibration model in the first vehicle test.

As can be seen from Figs. 12–17, all four calibration models can estimate the main error parameters of the PI-LDV. However, it should be noted that Figs. 13 and 16 show that the roll installation misalignment angle of PI-LDV cannot be

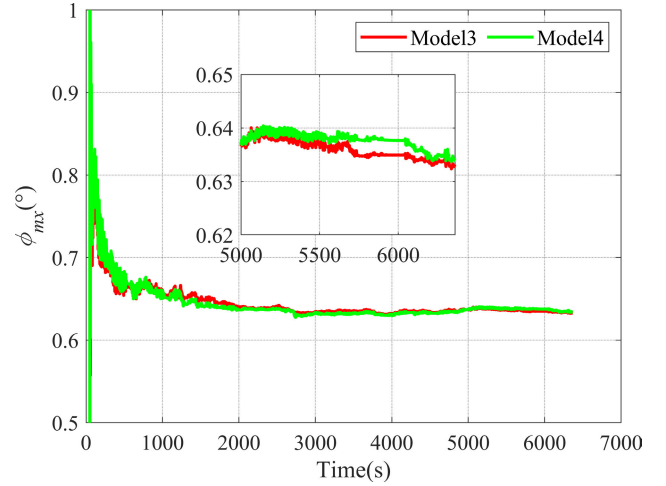


Fig. 15. Curve of the pitch installation misalignment angle in the first vehicle test.

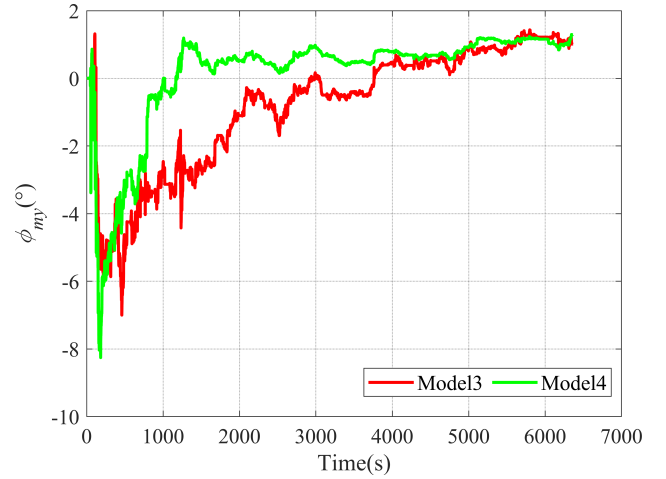


Fig. 16. Curve of the roll installation misalignment angle in the first vehicle test.

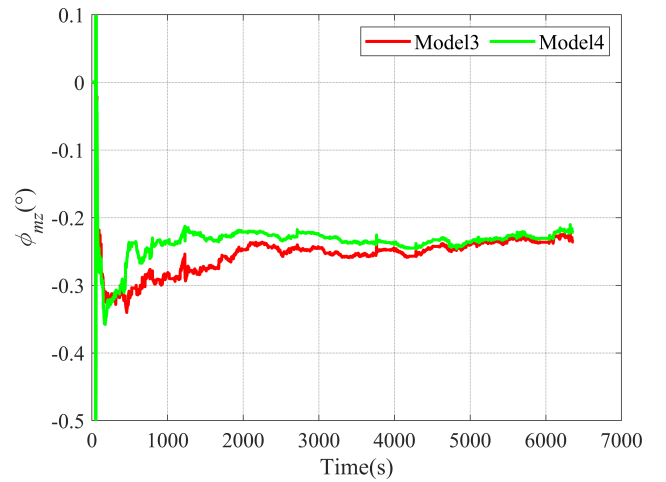


Fig. 17. Curve of the heading installation misalignment angle in the first vehicle test.

calibrated accurately. This is because the vehicle maneuvers on the y -axis are much larger than those on the x -axis and z -axis during the terrestrial vehicle test. As a result, the effect of

TABLE II
RESULTS OF STD FOR THREE MODELS IN THE FIRST TEST

	Time(s)	0~2000	2001~4000	4000~end
Model2	δK	0.0024	1.8996e-05	1.7235e-05
	ϕ_{mx}	0.0190	0.0031	0.0021
	ϕ_{mz}	0.0511	0.0069	0.0073
Model3	$\Delta\theta$	0.0624	6.2610e-05	5.4901e-05
	ϕ_{mx}	0.1152	0.0027	0.0018
	ϕ_{mz}	0.0756	0.0058	0.0084
Model4	$\Delta\theta$	0.0620	3.8461e-05	3.3890e-05
	ϕ_{mx}	0.1181	0.0036	0.0014
	ϕ_{mz}	0.0719	0.0053	0.0072

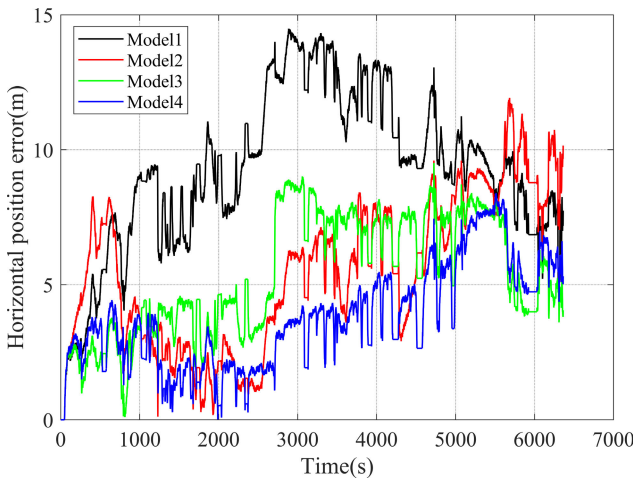


Fig. 18. First experiment's horizontal location error.

this error is ignored in this article. To compare the calibration performance of the three proposed models more specifically, their standard deviations (STDs) are shown in Table II.

Table II shows that within the time frame of 1–2000 s, Model 2 has the lowest STD value while Models 3 and 4 have similar STD values. These findings suggest that performing a coarse calibration before a filter calibration can accelerate the convergence speed. After 4000 s, all three models can converge the error term of PI-LDV to a relatively stable value. To judge the accuracy of the calibration results from all four models, the DR of the SINS/PI-LDV-integrated navigation system is performed using the calibration results. The horizontal and height positioning errors are shown in Figs. 18 and 19, respectively.

As shown in Figs. 18 and 19, the SINS/PI-LDV-integrated navigation system calibrated by Model 2, Model 3, and Model 4 has higher positioning accuracy than the one calibrated by Model 1, especially in terms of height. This indicates that using the two subvelocities of PI-LDV to obtain the 2-D velocity is better than using the compensated 1-D velocity of PI-LDV directly, and Model 2, Model 3, and Model 4 can calibrate the error parameters of the 2-D velocity accurately under their respective models. In addition, Model 3 and Model 4 have smaller horizontal positioning errors than Model 2 because

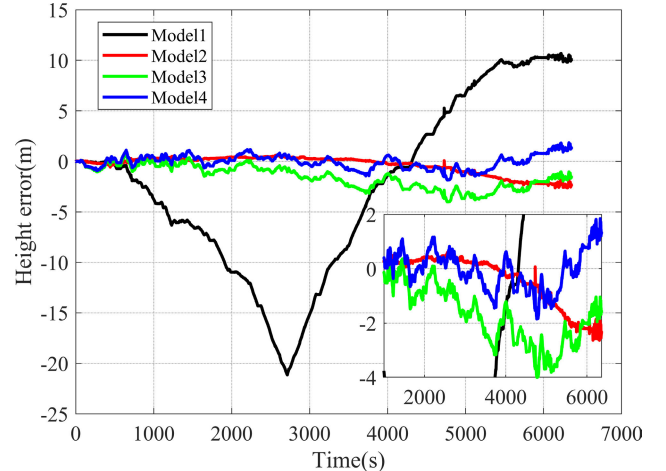


Fig. 19. First experiment's height positioning error.

TABLE III
RESULTS OF STD FOR THREE MODELS IN THE SECOND TEST

	Time(s)	0~2000	2001~4000	4000~end
Model2	δK	0.0041	2.2595e-05	2.8326e-05
	ϕ_{mx}	0.0282	0.0036	0.0022
	ϕ_{mz}	0.0466	0.0241	0.0117
Model3	$\Delta\theta$	0.0679	6.5925e-05	8.4130e-05
	ϕ_{mx}	0.1287	0.0032	0.0031
	ϕ_{mz}	0.0948	0.0072	0.0110
Model4	$\Delta\theta$	0.0621	6.9111e-05	7.3476e-05
	ϕ_{mx}	0.1212	0.0035	0.0028
	ϕ_{mz}	0.0659	0.0069	0.0078

the scale factor error in Model 2 is the combination of the velocity scale factor errors in the two directions of PI-LDV, and it does not estimate the scale factor error in each velocity direction accurately. It is also noteworthy that Model 4 has a slightly smaller error than Model 3. This is because Model 4 uses the two original velocities of PI-LDV directly instead of combining them into the 2-D velocities, thus avoiding some calibration error caused by the 2-D velocity error due to inaccurate measurement of a single beam.

To further verify the effectiveness and to evaluate the accuracy of the proposed calibration models in this article, the second vehicle test was carried out and the corresponding results are given directly in Figs. 20–28 and Table III.

As seen in Figs. 22–28 and Table III that four models have similar performance in the second experiment as that in the first experiment. This further demonstrates the superiority of the PI-LDV calibration models proposed in this article.

The horizontal location error and height positioning error of two independent tests are summarized in Table IV. In addition, the horizontal error ratios of two groups of field tests are shown in Fig. 29.

As shown in Table IV, compared to the traditional Model 1, Model 2 proposed in this article improves horizontal positioning accuracy by 17.7% and 28.7%, respectively, in two

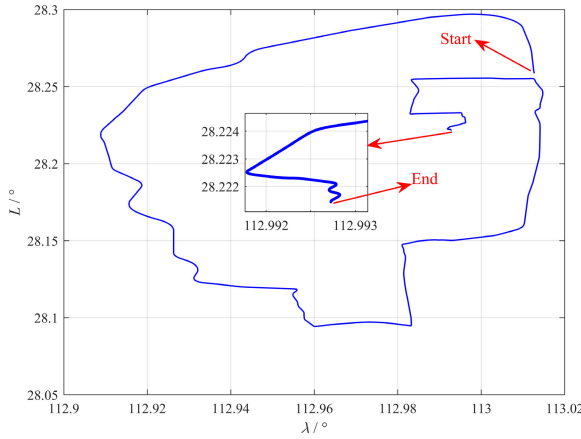


Fig. 20. Trajectory of the vehicle in the second field test.

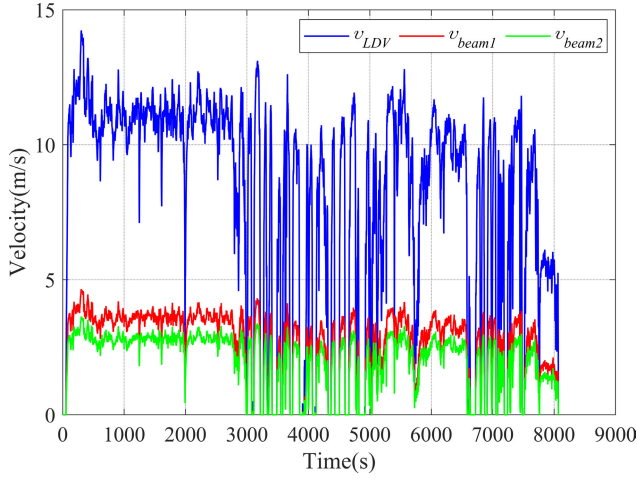


Fig. 21. Velocity curve of PI-LDV output in the second field test.

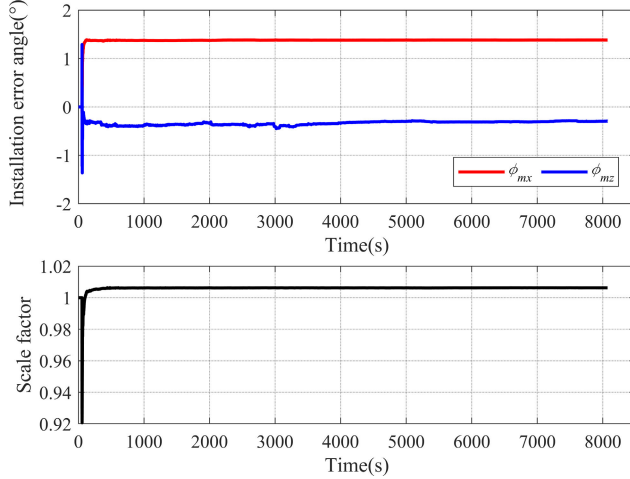


Fig. 22. Calibration results for the traditional calibration model in the second field test.

tests. Similarly, Model 3 improves horizontal positioning accuracy by 34.3% and 49.0%, while Model 4 improves it by 42.0% and 53.2%. The horizontal error rates for both groups of experiments shown in Fig. 29 further demonstrate the effectiveness of the three models proposed in this article. The height positioning results are also clear: Models 2, 3,

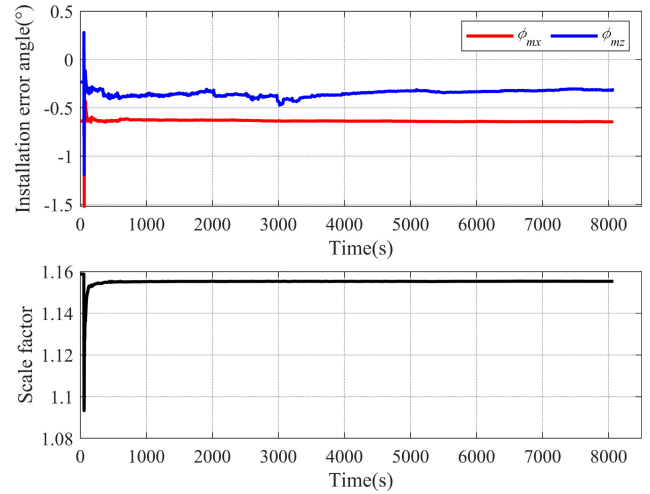


Fig. 23. Calibration results for the loosely integrated calibration model in the second field test.

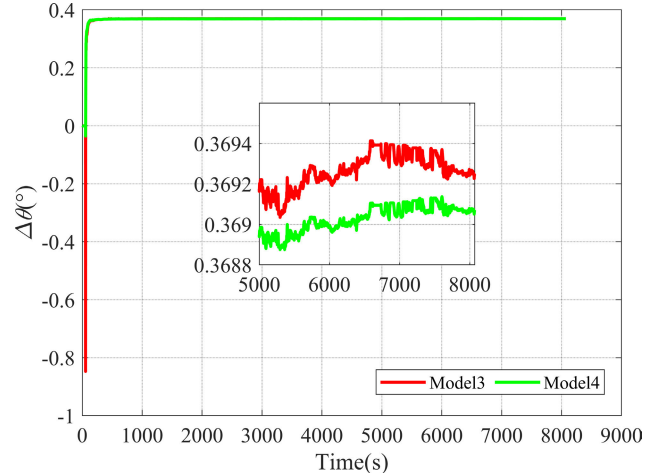
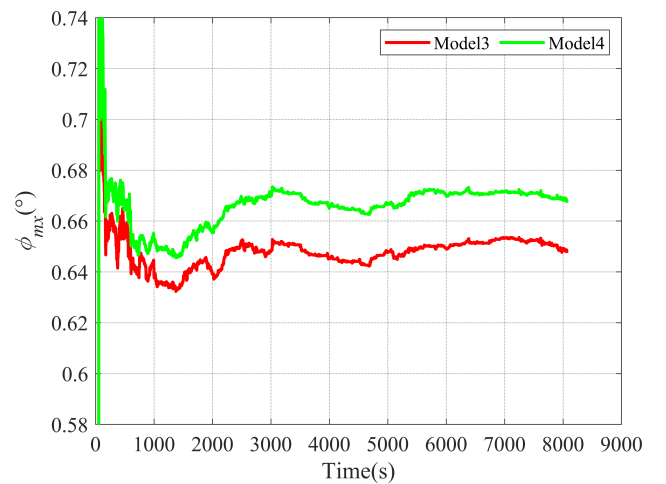
Fig. 24. Curve of the $\Delta\theta$ for the tightly integrated calibration model and the ultratightly integrated calibration model in the second vehicle test.

Fig. 25. Curve of the pitch installation misalignment angle in the second vehicle test.

and 4 all show significant improvement compared to the traditional Model 1 with an error of less than 6 m. Therefore, the three calibration models based on two subvelocities of

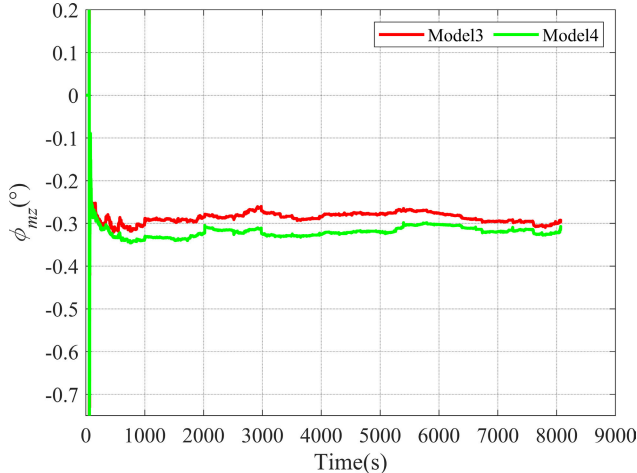


Fig. 26. Curve of the heading installation misalignment angle in the second vehicle test.

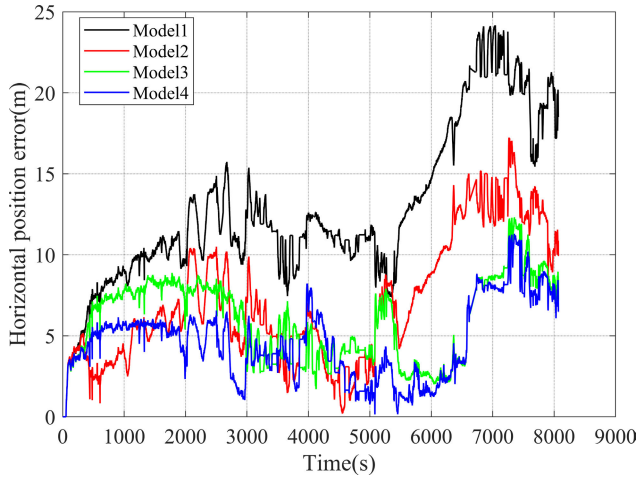


Fig. 27. Second experiment's horizontal location error.

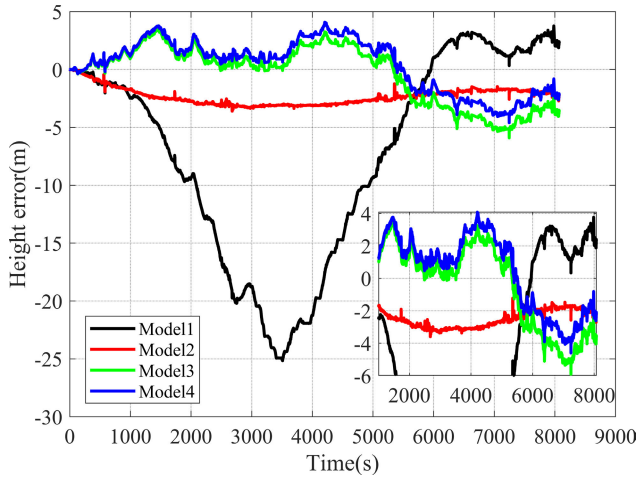


Fig. 28. Second experiment's height positioning error.

PI-LDV proposed in this article are superior to the traditional calibration model based on the 1-D velocity output of PI-LDV. Moreover, compared to Models 2 and 3, Model 4 has the highest horizontal positioning accuracy and nearly optimal height positioning accuracy.

TABLE IV
MAX OF THE POSITION ERROR (METERS)

Models		Test 1 (51.69km)	Test 2 (65.34km)
	Horizontal error	14.486	24.161
Model1	Height error	-21.143	-25.161
	Horizontal error	11.925	17.234
Model2	Height error	-2.632	-3.598
	Horizontal error	9.512	12.315
Model3	Height error	-4.018	-5.909
	Horizontal error	8.399	11.299
Model4	Height error	-1.851	-4.301
	Horizontal error		

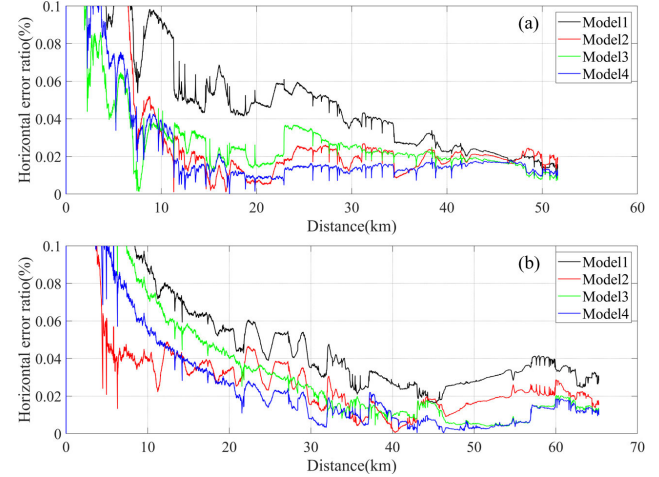


Fig. 29. (a) First experiment's horizontal error ratio. (b) Second experiment's horizontal error ratio.

V. CONCLUSION

This article proposes three calibration models based on the two subvelocities of PI-LDV, aiming at the problem that PI-LDV is used as 1-D-LDV in the field of integrated navigation. By using the proposed calibration models, PI-LDV can obtain accurate 2-D velocity, which can greatly improve the height estimation accuracy of the SINS/PI-LDV-integrated navigation system. Two groups of vehicle field tests verify the validity of the proposed calibration models. The results show that the proposed calibration models can improve the positioning accuracy, especially the height estimation accuracy, of the SINS/PI-LDV-integrated navigation system, which provides an important reference value for the application of PI-LDV in land navigation.

Although the method proposed in this article can fully utilize the structural advantages of PI-LDV, it is still limited by the optical path structure. Specifically, PI-LDV cannot provide the lateral velocity of the vehicle, which makes it unable to cope with vehicle sideslip. For future research, 3-D-LDV and the combination of multiple PI-LDVs are expected to enable the land SINS/LDV-integrated navigation system to handle various maneuvers of the vehicle. Moreover, the impact of LDV temperature on the SINS/LDV-integrated navigation system will also be a focus of future work.

REFERENCES

- [1] C. Gao, Q. Wang, G. Wei, and X. Long, "A highly accurate calibration method for terrestrial laser Doppler velocimeter," *IEEE Trans. Instrum. Meas.*, vol. 66, no. 8, pp. 1994–2003, Aug. 2017.

- [2] A. Tal, I. Klein, and R. Katz, "Inertial navigation system/Doppler velocity log (INS/DVL) fusion with partial DVL measurements," *Sensors*, vol. 17, no. 2, p. 415, Feb. 2017.
- [3] M. Wang, W. Wu, X. He, Y. Li, and X. Pan, "Consistent ST-EKF for long distance land vehicle navigation based on SINS/OD integration," *IEEE Trans. Veh. Technol.*, vol. 68, no. 11, pp. 10525–10534, Nov. 2019.
- [4] B. Xu, L. Wang, S. Li, and J. Zhang, "A novel calibration method of SINS/DVL integration navigation system based on quaternion," *IEEE Sensors J.*, vol. 20, no. 16, pp. 9567–9580, Aug. 2020.
- [5] W. Ouyang, Y. Wu, and H. Chen, "INS/Odometer land navigation by accurate measurement modeling and multiple-model adaptive estimation," *IEEE Trans. Aerosp. Electron. Syst.*, vol. 57, no. 1, pp. 245–262, Feb. 2021.
- [6] S. Du, Y. Huang, B. Lin, J. Qian, and Y. Zhang, "A lie group manifold-based nonlinear estimation algorithm and its application to low-accuracy SINS/GNSS integrated navigation," *IEEE Trans. Instrum. Meas.*, vol. 71, pp. 1–27, 2022.
- [7] L. Chang, Y. Li, and B. Xue, "Initial alignment for a Doppler velocity log-aided strapdown inertial navigation system with limited information," *IEEE/ASME Trans. Mechatronics*, vol. 22, no. 1, pp. 329–338, Feb. 2017.
- [8] D. Wang, B. Wang, H. Huang, and Y. Yao, "Online calibration method of DVL error based on improved integrated navigation model," *IEEE Sensors J.*, vol. 22, no. 21, pp. 21082–21092, Nov. 2022.
- [9] V. Girbés-Juan, L. Armesto, D. Hernández-Ferrández, J. F. Dols, and A. Sala, "Asynchronous sensor fusion of GPS, IMU and CAN-based odometry for heavy-duty vehicles," *IEEE Trans. Veh. Technol.*, vol. 70, no. 9, pp. 8617–8626, Sep. 2021.
- [10] Z. Wen, G. Yang, Q. Cai, and T. Chen, "A novel Bluetooth-odometer-Aided smartphone-based vehicular navigation in satellite-denied environments," *IEEE Trans. Ind. Electron.*, vol. 70, no. 3, pp. 3136–3146, Mar. 2023.
- [11] H. Zhao, L. Miao, and H. Shao, "Adaptive two-stage Kalman filter for SINS/odometer integrated navigation systems," *J. Navigat.*, vol. 70, no. 2, pp. 242–261, Mar. 2017.
- [12] X. Nie and J. Zhou, "Pitch independent vehicle-based laser Doppler velocimeter," *Opt. Lasers Eng.*, vol. 131, Aug. 2020, Art. no. 106072.
- [13] Z. Jian and L. Xingwu, "Research on laser Doppler velocimeter for vehicle self-contained inertial navigation system," *Opt. Laser Technol.*, vol. 42, no. 3, pp. 477–483, Apr. 2010.
- [14] J. Zhou, X. Nie, and J. Lin, "A novel laser Doppler velocimeter and its integrated navigation system with strapdown inertial navigation," *Opt. Laser Technol.*, vol. 64, pp. 319–323, Dec. 2014.
- [15] X. Zhang, Z. Lin, and C. Zhang, "Autonomous integrated navigation method based on the strapdown inertial navigation system and LiDAR," *Opt. Eng.*, vol. 53, no. 7, Jul. 2014, Art. no. 074112.
- [16] X. Zhang, J. Yin, Z. Lin, and C. Zhang, "A positioning and orientation method based on the usage of INS and single-beam LiDAR," *Optik*, vol. 126, no. 22, pp. 3376–3381, Nov. 2015.
- [17] X. Zhang, H. Shi, J. Pan, and C. Zhang, "Integrated navigation method based on inertial navigation system and LiDAR," *Opt. Eng.*, vol. 55, no. 4, Apr. 2016, Art. no. 044102.
- [18] Q. Fu, Y. Liu, Z. Liu, S. Li, and B. Guan, "High-accuracy SINS/LDV integration for long-distance land navigation," *IEEE/ASME Trans. Mechatronics*, vol. 23, no. 6, pp. 2952–2962, Dec. 2018.
- [19] P. Wang, Q. Zhong, L. Tan, and Y. Zhang, "Design of SINS/LDV/OD autonomous positioning system based on carrier constraints," *J. Phys. Conf. Ser.*, vol. 1176, no. 5, pp. 1–14, Sep. 2019.
- [20] B. Yang, L. Xue, H. Fan, and X. Yang, "SINS/odometer/Doppler radar high-precision integrated navigation method for land vehicle," *IEEE Sensors J.*, vol. 21, no. 13, pp. 15090–15100, Jul. 2021.
- [21] Q. Wang, X. Nie, C. Gao, J. Zhou, G. Wei, and X. Long, "Calibration of a three-dimensional laser Doppler velocimeter in a land integrated navigation system," *Appl. Opt.*, vol. 57, no. 29, p. 8566, Oct. 2018.
- [22] Q. Wang, C. Gao, J. Zhou, G. Wei, X. Nie, and X. Long, "Two-dimensional laser Doppler velocimeter and its integrated navigation with a strapdown inertial navigation system," *Appl. Opt.*, vol. 57, no. 13, p. 3334, May 2018.
- [23] Z. Xiang, Q. Wang, R. Huang, C. Xi, X. Nie, and J. Zhou, "Position observation-based calibration method for an LDV/SINS integrated navigation system," *Appl. Opt.*, vol. 60, no. 26, p. 7869, Sep. 2021.
- [24] C. Xi et al., "Online calibration technology for a one-dimensional laser Doppler velocimeter based on a strapdown inertial navigation system," *Appl. Opt.*, vol. 61, no. 5, p. 1229, Feb. 2022.
- [25] Y. Zhu, X. Wang, J. Zheng, H. Xiong, and Y. Zhao, "Using GPS time-differenced carrier phase observations to calibrate LDV/INS integrated navigation systems," *IEEE Sensors J.*, vol. 20, no. 1, pp. 405–414, Jan. 2020.
- [26] R. Huang, Q. Wang, X. Nie, and J. Zhou, "One-dimensional reference-beam LDV for accurate altitude estimation in a land vehicle," *Appl. Opt.*, vol. 59, no. 34, pp. 10667–10672, Dec. 2020.
- [27] M. Wang, J. Cui, Y. Huang, W. Wu, and X. Du, "Schmidt ST-EKF for autonomous land vehicle SINS/ODO/LDV integrated navigation," *IEEE Trans. Instrum. Meas.*, vol. 70, pp. 1–9, 2021.
- [28] Z. Xiang, Q. Wang, R. Huang, C. Xi, X. Nie, and J. Zhou, "In-motion initial alignment method for a laser Doppler velocimeter-aided strapdown inertial navigation system based on an adaptive unscented quaternion H-infinite filter," *Meas. Sci. Technol.*, vol. 33, no. 3, Mar. 2022, Art. no. 035001.
- [29] Z. Xiang, Q. Wang, R. Huang, C. Xi, X. Nie, and J. Zhou, "A fast robust in-motion alignment method for laser Doppler velocimeter-aided strapdown inertial navigation system," *IEEE Sensors J.*, vol. 22, no. 17, pp. 17254–17265, Sep. 2022.
- [30] D. H. Titterton, J. L. Weston, and J. L. Weston, *Strapdown Inertial Navigation Technology*. London, U.K.: Peter Peregrinus Limited, 1997.

Zhiyi Xiang received the M.E. degree from the College of Advanced Interdisciplinary Studies, National University of Defense Technology, Changsha, China, in 2021, where he is currently pursuing the Ph.D. degree.

His current research interest is SINS/LDV-integrated navigation technology.

Qi Wang received the M.E. degree from the College of Optoelectronic Science and Engineering, National University of Defense Technology, Changsha, China, in 2013, and the Ph.D. degree from the College of Advanced Interdisciplinary Studies, National University of Defense Technology, in 2018.

He is currently an Associate Professor with the College of Advanced Interdisciplinary Studies, National University of Defense Technology. His interests include the laser Doppler velocimetry and SINS/LDV-integrated navigation technology.

Rong Huang received the M.E. degree from the College of Advanced Interdisciplinary Studies, National University of Defense Technology, Changsha, China, in 2019, where she is currently pursuing the Ph.D. degree.

Her current research interests include the laser Doppler velocimetry and SINS/LDV-integrated navigation technology.

Shilong Jin received the M.E. and Ph.D. degrees from the College of Optoelectronic Science and Engineering, National University of Defense Technology, Changsha, China, in 1994 and 2006, respectively.

He is currently a Professor with the College of Advanced Interdisciplinary Studies, National University of Defense Technology. His interests include opto-electronic detection technology and inertial sensors and systems.

Xiaoming Nie received the M.E. and Ph.D. degrees from the College of Optoelectronic Science and Engineering, National University of Defense Technology, Changsha, China, in 2010 and 2014, respectively.

He is currently an Associate Professor with the College of Advanced Interdisciplinary Studies, National University of Defense Technology. His interests include the optoelectronic velocimetry, laser Doppler velocimetry, and SINS/LDV-integrated navigation technology.

Jian Zhou received the B.E. and Ph.D. degrees from the College of Optoelectronic Science and Engineering, National University of Defense Technology, Changsha, China, in 2006 and 2011, respectively.

He is currently an Associate Professor with the College of Advanced Interdisciplinary Studies, National University of Defense Technology. His interests include the optoelectronic velocimetry, laser Doppler velocimetry, and SINS/LDV-integrated navigation technology.